Editors' Suggestion

Trapped-Ion Spin-Motion Coupling with Microwaves and a Near-Motional Oscillating Magnetic Field Gradient

R. Srinivas,[1,2,*] S. C. Burd,[1,2] R. T. Sutherland,[3] A. C. Wilson,[1] D. J. Wineland,[1,2,4] D. Leibfried,[1] D. T. C. Allcock,[1,2,4] and D. H. Slichter[1,†]

[1]*Time and Frequency Division, National Institute of Standards and Technology, 325 Broadway, Boulder, Colorado 80305, USA*
[2]*Department of Physics, University of Colorado, Boulder, Colorado 80309, USA*
[3]*Physics Division, Physical and Life Sciences, Lawrence Livermore National Laboratory, Livermore, California 94550, USA*
[4]*Department of Physics, University of Oregon, Eugene, Oregon 97403, USA*

(Received 17 December 2018; published 26 April 2019)

We present a new method of spin-motion coupling for trapped ions using microwaves and a magnetic field gradient oscillating close to the ions' motional frequency. We demonstrate and characterize this coupling experimentally using a single ion in a surface-electrode trap that incorporates current-carrying electrodes to generate the microwave field and the oscillating magnetic field gradient. Using this method, we perform resolved-sideband cooling of a single motional mode to its ground state.

DOI: 10.1103/PhysRevLett.122.163201

Coupling the internal spin states of trapped ions to their motion is essential for applications in quantum information processing, quantum simulation, and metrology [1–3], such as quantum logic gates [4,5], simulations of many-body spin systems [6–8], and quantum logic spectroscopy for optical clocks [9] and molecules [10]. This coupling requires a field gradient across the ions' wave function, and is usually accomplished using laser-induced interactions. However, photon scattering errors are a fundamental limit for laser-based spin-motion coupling [11], and are the leading error in the highest-fidelity quantum logic gates [12,13]. Laser-induced coupling is also sensitive to fluctuations in the optical phase and intensity at the ion, which can be experimentally demanding to mitigate. Alternative laser-free methods, which are not limited by photon scattering and offer improved phase and amplitude stability, use microwave radiation and magnetic field gradients to perform the spin-motion coupling. These fields and gradients can be generated using current-carrying wires integrated in a surface-electrode trap [14], a promising platform for large scale quantum computing or simulation with ions. The integrated microwave circuitry can also be used to perform high-fidelity single-qubit gates [15,16] and individual ion addressing [17,18].

Laser-free spin-motion coupling has been proposed and demonstrated using either a static magnetic field gradient with separate microwave fields [19–21] or oscillating magnetic field gradients close to the qubit frequency [22,23]. High-fidelity two-qubit gates have been performed with these methods [24,25]. However, the near-qubit oscillating gradient method requires large currents near the qubit frequency to generate a strong gradient, which can be technically challenging for typical gigahertz-frequency hyperfine qubits. Furthermore, most entangling gates require multiple such currents at different frequencies in the same trap electrodes. In contrast, the static gradient scheme enables multiple interactions to be generated using only a single strong gradient with multiple weak microwave fields. However, the spin-motion coupling strength for this scheme decreases rapidly with increasing motional frequency for a given microwave current. Higher motional frequencies are desirable to mitigate the effects of anomalous heating [26] and to reduce the average phonon occupation of the motional modes after Doppler cooling. This reduces the time for ground-state cooling, a requirement for many quantum information and simulation experiments.

In this work, we demonstrate a new technique for spin-motion coupling in trapped ions using microwaves and a near-field magnetic field gradient oscillating close to the ions' motional frequency. This method is a generalization of the static-gradient scheme, and enables stronger spin-motion coupling for a given motional frequency, gradient strength, and microwave field amplitude. In particular, strong spin-motion coupling with low microwave power can be maintained even at high motional frequencies. This near-motional gradient can be more efficiently generated than an equivalent gigahertz-frequency gradient, and only one strong gradient is required to implement multiple simultaneous spin-motion coupling interactions. Here, we characterize the spin-motion coupling strength by tuning the microwave and gradient parameters and identify optimal working regimes. We cool an ion to its motional ground state as a proof of principle.

The physics underlying this spin-motion coupling involves a magnetic field gradient which causes a spin-dependent spatial displacement of the ion. We consider the case of a microwave-frequency hyperfine qubit, but in

general this would apply to any two-level system, as long as the gradient displaces one of the qubit states relative to the other. The basic physics has been observed previously using the intensity gradient from a running optical lattice [27], but with the aforementioned limitations of a laser-based approach. The harmonically confined ion has internal "spin" states labeled $|\downarrow\rangle$ and $|\uparrow\rangle$, separated in energy by $\hbar\omega_0$, as well as motional states $|n\rangle$ separated by $\hbar\omega_r$. In the absence of any spin-dependent displacement, a microwave field driving the $|\downarrow\rangle \leftrightarrow |\uparrow\rangle$ transition can only drive spin flips that leave the ion's motional state unchanged ($\Delta n = 0$). However, if a gradient displaces $|\uparrow\rangle$ relative to $|\downarrow\rangle$ [see Fig. 1(a)], the overlap between their corresponding motional state wave functions is modified, enabling a microwave field with detuning $\delta = \pm\omega_r$ from the qubit frequency ω_0 to drive motion-changing sideband transitions ($\Delta n = \pm 1$); this can be viewed as a change in the Franck-Condon factors [28,29]. For small displacements, the sideband Rabi frequency increases with the magnitude of the displacement Δx, and for a static gradient, the explicit dependence of the sideband Rabi frequency on the motional frequency is $\Omega_{\mathrm{sb}} \propto \omega_r^{-3/2}$. If the gradient is instead oscillating at a frequency ω_g, the spin-dependent displacement Δx_g can be larger for a given

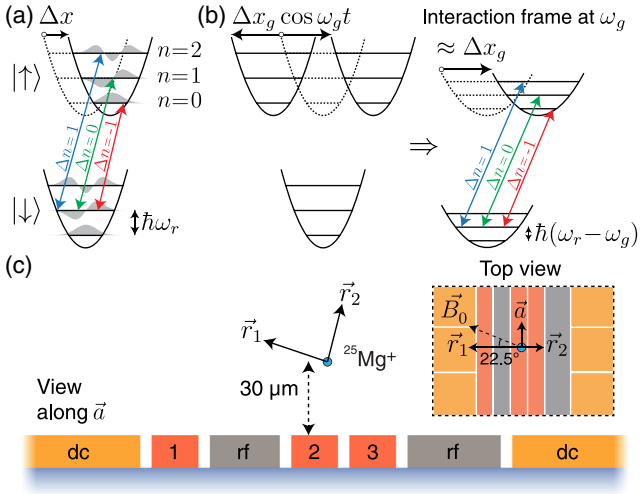

FIG. 1. Schematic description of a qubit coupled to a harmonic oscillator with a spin-dependent displacement from (a) a static gradient or (b) an oscillating gradient. An additional microwave field drives $|\downarrow\rangle \leftrightarrow |\uparrow\rangle$ transitions. (a) For a static gradient, detuning the microwave field by $\pm\omega_r$ drives sideband transitions with $\Delta n = \pm 1$. (b) An oscillating gradient at ω_g is formally equivalent to a static gradient in the interaction frame oscillating at ω_g, ignoring fast-oscillating terms. The sideband transitions now occur at detunings $\pm(\omega_r - \omega_g)$. (c) Schematic of the surface electrode trap. The ion has three motional modes: $\vec{a}$ along the trap axis and $\vec{r}_1$ and $\vec{r}_2$ perpendicular to the trap axis. The dc and rf electrodes provide trapping potentials, while oscillating currents in electrodes 1, 2, and 3 generate magnetic fields and magnetic field gradients at the ion. A static magnetic field $\vec{B}_0$ parallel to the plane of the trap defines the quantization axis $\hat{z}$.

gradient strength if the ion motion is being driven closer to resonance [30], as shown in Fig. 1(b). Sideband transitions now occur at $\delta = \pm(\omega_r - \omega_g)$, made apparent by transforming into an interaction frame oscillating at ω_g and making a rotating wave approximation. The gradient in this frame appears static, with a modified "motional frequency" $(\omega_r - \omega_g)$. The sideband Rabi frequency scales as $\Omega_{\mathrm{sb}} \propto [\sqrt{\omega_r}(\omega_r - \omega_g)]^{-1}$, which grows larger as $\omega_g \to \omega_r$, and reduces to the static-gradient case when $\omega_g = 0$. Thus the spin-motion coupling strength can be larger than the static gradient case for a given ω_r, gradient strength, and microwave field amplitude. An additional, weaker set of sidebands (highlighted by transforming into an interaction frame oscillating at $-\omega_g$ instead) appears at $\delta = \pm(\omega_r + \omega_g)$, with $\Omega_{\mathrm{sb}} \propto [\sqrt{\omega_r}(\omega_r + \omega_g)]^{-1}$.

The system Hamiltonian $\hat{H}(t)$ with fields oscillating at ω_g and $\omega_0 + \delta$ can be written in the interaction picture with respect to $\hat{H}_0 = (\hbar\omega_0/2)\hat{\sigma}_z + \hbar\omega_g\hat{a}^\dagger\hat{a}$ as

$$\begin{aligned}\hat{H}_I(t) = {} & \hbar\Omega_g\hat{\sigma}_z[(\hat{a}+\hat{a}^\dagger) + (\hat{a}e^{-2i\omega_g t} + \hat{a}^\dagger e^{2i\omega_g t})] \\ & + 2\hbar\Omega_z\cos(\omega_g t)\hat{\sigma}_z + \hbar(\omega_r - \omega_g)\hat{a}^\dagger\hat{a} \\ & + \hbar\Omega_\mu(\hat{\sigma}_+ e^{-i\delta t} + \hat{\sigma}_- e^{i\delta t}), \end{aligned} \tag{1}$$

where $\hat{\sigma}_z = |\uparrow\rangle\langle\uparrow| - |\downarrow\rangle\langle\downarrow|$, $\hat{\sigma}_+ = |\uparrow\rangle\langle\downarrow|$, $\hat{\sigma}_- = |\downarrow\rangle\langle\uparrow|$, and $\hat{a}^\dagger$ and $\hat{a}$ are creation and annihilation operators for the ion motion. The coupling of the qubit states by the microwave field is characterized by Ω_μ [31]. The spin and motion are coupled (with strength $\propto \Omega_g$) by the gradient of a magnetic field B_g along the quantization axis oscillating at ω_g. In this interaction frame, ignoring faster terms at $2\omega_g$, the gradient appears static with a modified "motional frequency" $\omega_r - \omega_g$. In general, B_g is nonzero at the ion position, giving an additional term in the Hamiltonian proportional to Ω_z. We define Ω_g and Ω_z as

$$\begin{aligned}\Omega_g &\equiv \frac{r_0(\hat{r}\cdot\nabla B_g)}{4}\frac{d\omega_0}{dB_z}\bigg|_{B_z=|\vec{B}_0|}, \\ \Omega_z &\equiv \frac{B_g}{4}\frac{d\omega_0}{dB_z}\bigg|_{B_z=|\vec{B}_0|}. \end{aligned} \tag{2}$$

The sensitivity of the qubit frequency ω_0 to changes in the magnetic field B_z along the quantization axis $\hat{z}$ (defined by a static magnetic field $\vec{B}_0$) is described by $d\omega_0/dB_z$, and $r_0 = \sqrt{\hbar/2M\omega_r}$ is the ground-state extent of the ion wave function for the motional mode along the $\hat{r}$ direction for ion mass M. This gives an implicit $\omega_r^{-1/2}$ dependence to Ω_g.

By transforming Eq. (1) into the interaction picture with respect to the terms in the first two lines [31], different interactions are obtained for specific values of δ. Sideband transitions occur at $\delta = \pm(\omega_r - \omega_g)$ or $\delta = \pm(\omega_r + \omega_g)$. For the first case, the Hamiltonian is given by

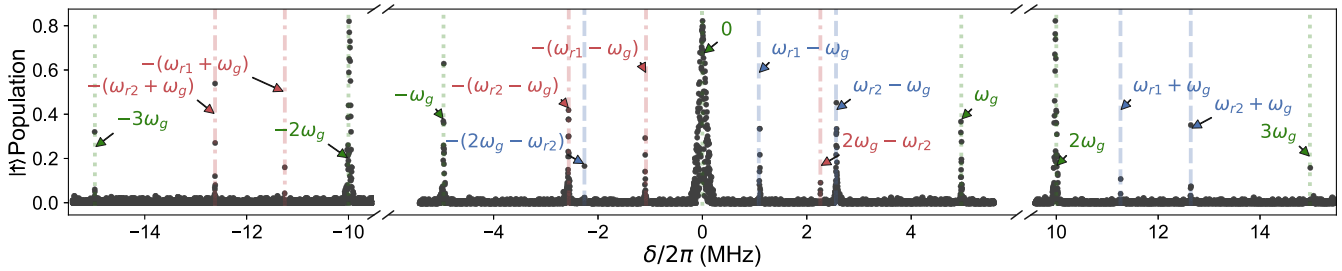

FIG. 2. Microwave spectroscopy in the presence of a magnetic field with a gradient oscillating at $\omega_g/2\pi = 5$ MHz. Trap radial frequencies are $(\omega_{r_1}, \omega_{r_2})/2\pi \approx (6.2, 7.6)$ MHz. An additional microwave pulse with detuning δ from the qubit frequency is applied for 500 μs. The ion is initialized close to the Doppler temperature in the $|\downarrow\rangle$ state, and the population in the $|\uparrow\rangle$ state is measured at the end of the pulse. Spin-flip transitions with $\Delta n = 0$ (green dotted lines) occur when $\delta = \pm m\omega_g$, and blue (red) motional sideband transitions with $\Delta n = 1$ ($\Delta n = -1$) [blue dashed (red dash-dotted) lines] occur when $\delta = +(\omega_{ri} \pm \omega_g)$ [$\delta = -(\omega_{ri} \pm \omega_g)$]. Weak sideband transitions at $\pm(\omega_{r2} - 2\omega_g)$ correspond to higher-order interactions [31]. Population error bars are omitted for clarity.

$$\hat{H}_{\mathrm{sb}} = \pm\hbar\Omega_{\mathrm{sb}}(\hat{\sigma}_{\pm}\hat{a}^{\dagger} + \hat{\sigma}_{\mp}\hat{a}), \tag{3}$$

where the upper (lower) sign choice corresponds to the blue (red) sideband interaction. The sideband Rabi frequency is $\Omega_{\mathrm{sb}} \equiv 2\Omega_g\Omega_\mu/(\omega_r - \omega_g)J_0(4\Omega_z/\omega_g)$, where J_0 is the zeroth-order Bessel function of the first kind. For the case $\delta = \omega_r + \omega_g$, the denominator $\omega_r - \omega_g$ in Ω_{sb} is replaced by $\omega_r + \omega_g$. The Rabi frequency Ω_{sb} is maximized when the argument of $J_0(4\Omega_z/\omega_g)$ is zero, which corresponds to $B_g = 0$ (importantly, this does not imply $\nabla B_g = 0$). When B_g is nonzero, the qubit frequency is modulated, enabling spin-flip transitions that do not change the motional state of the ion. These transitions occur when $\delta = m\omega_g$ for integer m, and the resulting Hamiltonian is

$$\hat{H}_m = \hbar\Omega_m\hat{\sigma}_x, \tag{4}$$

where $\Omega_m \equiv \Omega_\mu J_m(4\Omega_z/\omega_g)$ is the spin-flip Rabi frequency, and J_m is the mth-order Bessel function of the first kind. A similar effect has been observed from residual magnetic fields generated by the rf trapping potentials [32].

In our experiment, the gradient and microwave fields are generated by currents driven through electroplated gold electrodes of a cryogenic (18 K) linear surface-electrode Paul trap, labeled as electrodes 1, 2, and 3 in Fig. 1(c). A single $^{25}Mg^+$ ion is trapped ≈30 μm above the surface with motional frequencies $(\omega_a, \omega_{r_1}, \omega_{r_2})/2\pi \approx (3.2, 6.2, 7.6)$ MHz, where $\vec{a}$ is along the axis of the trap, and $\vec{r}_1, \vec{r}_2$ lie in the radial plane. We use the $|F = 3, m_F = 3\rangle \equiv |\downarrow\rangle$ and $|F = 2, m_F = 2\rangle \equiv |\uparrow\rangle$ states within the $3^2S_{1/2}$ hyperfine manifold as our qubit, which has a transition frequency of $\omega_0/2\pi = 1.326$ GHz in the externally applied magnetic field $|\vec{B}_0| = 21.3$ mT. The magnetic field sensitivity of this transition is $(d\omega_0/dB_z)/2\pi = -19.7$ MHz/mT, and the magnitude of the static field gives ∼100 MHz of spectral separation between adjacent Zeeman sublevels. We prepare $|\downarrow\rangle$ by optical pumping on the $3^2S_{1/2} \leftrightarrow 3^2P_{3/2}$ transition at 280 nm with σ^+ polarized light. The qubit is read out by detecting fluorescence from the laser-driven $|\downarrow\rangle \leftrightarrow |3^2P_{3/2}, F = 4, m_F = 4\rangle$ cycling transition. Before detection, microwave pulses are used to shelve $|\uparrow\rangle$ to the far-detuned $|3^2S_{1/2}, F = 2, m_F = -1\rangle$ state. To realize spin-motion coupling, we apply simultaneous currents (which are ramped on and off over 10 μs) to the trap electrodes at two frequencies, ω_g and $\omega_0 + \delta$. We apply up to 0.5(1) A rms per electrode at $\omega_g/2\pi = 5$ MHz, corresponding to 6(1) mW of dissipation in the trap; dissipation from the drive at $\omega_0 + \delta$ is $\ll$1 mW [31].

With the oscillating gradient applied, we perform microwave spectroscopy by varying δ as shown in Fig. 2. Spin-flip transitions occur at $\delta = m\omega_g$ since $B_g \neq 0$ for this experiment, and motional sideband transitions appear at $\delta = \pm(\omega_{ri} - \omega_g)$ and $\delta = \pm(\omega_{ri} + \omega_g)$, where ω_{ri} is the frequency of the radial mode $\vec{r}_1$ or $\vec{r}_2$. Weak higher-order sidebands are also visible [31]. We do not see sideband transitions for the axial mode $\vec{a}$ as the gradient along the trap axis is (by design) very small. Following Eq. (4), the spin-flip transitions are characterized by measuring the Rabi frequencies Ω_m as a function of B_g. The values of Ω_m versus B_g are shown for $m = \{0, 1, 2, 3, 4, 5\}$ in Fig. 3.

Setting B_g, and hence Ω_z, to zero maximizes Ω_{sb} for the sideband transitions described in Eq. (3); at this point, Ω_{sb} is insensitive to variations in B_g to first order. We set $B_g = 0$ by adjusting the relative phases and amplitudes of currents oscillating at ω_g in electrodes 1, 2, and 3 to minimize $\Omega_{m=1}$, which is proportional to B_g as $B_g \to 0$. The magnitude of Ω_{sb} is insensitive to components of the oscillating magnetic field perpendicular to $\vec{B}_0$, which produce an ac Zeeman shift on the qubit of less than 100 kHz.

The sideband Rabi frequency also depends on the microwave Rabi frequency Ω_μ with $\Omega_{\mathrm{sb}} \propto 2\Omega_\mu/(\omega_r - \omega_g)$. Because of the ac Zeeman shift from the microwave [31], the detunings required for the sidebands are shifted from $\delta = \pm(\omega_r - \omega_g)$ to

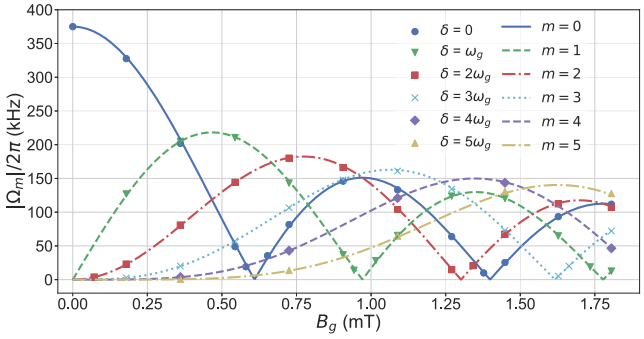

FIG. 3. Dependence of the spin-flip Rabi frequency Ω_m on B_g. Here, we apply a current of variable amplitude oscillating at ω_g to electrode 2 in addition to a microwave field with detuning δ and Rabi frequency $\Omega_\mu/2\pi = 375$ kHz. Spin-flip transitions occur when $\delta = m\omega_g$ with $\Omega_m = \Omega_\mu J_m(4\Omega_z/\omega_g)$, where $\Omega_z \propto B_g$. We calibrate the horizontal axis scale by fitting the data for $\delta = 0$ to $|J_0(4\Omega_z/\omega_g)|$. The theory curves (dashed) for $m > 0$ have no adjustable parameters. Error bars are smaller than the data points.

$$\delta \to \pm\sqrt{(\omega_r - \omega_g)^2 - 4\Omega_\mu^2}. \tag{5}$$

Thus, as $2\Omega_\mu$ approaches $\omega_r - \omega_g$, δ approaches zero, causing the microwave field required for the sideband to drive spin flips resonantly. This sets a limit for the maximum usable Ω_μ for driving sidebands. Operating close to this limit requires careful microwave pulse shaping to minimize off-resonant qubit excitation. We experimentally verify the relationship of both Ω_{sb} and the ac Zeeman shift to Ω_μ as shown in Fig. 4(a). We determine Ω_{sb} by cooling the r_1 mode to its ground state and driving the blue sideband transition. We set $(\omega_{r1} - \omega_g)/2\pi \approx 1.2$ MHz and vary $2\Omega_\mu/2\pi$ from 0 to 1.1 MHz. A linear fit to the

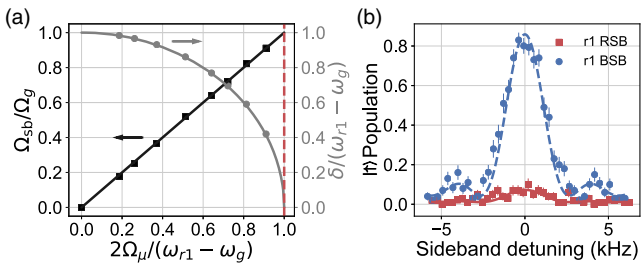

FIG. 4. Sideband characterization. (a) The normalized blue sideband Rabi frequency Ω_{sb}/Ω_g (black squares, left axis) and the normalized microwave detuning $\delta/(\omega_{r1} - \omega_g)$ from Eq. (5) (gray circles, right axis) are plotted as a function of $2\Omega_\mu/(\omega_{r1} - \omega_g)$. Error bars are smaller than the data points. The red dashed line denotes the limit on Ω_μ described in the text. The black line is a linear fit to the data; the gray line is a theoretical plot of Eq. (5). (b) Populations in $|\uparrow\rangle$ after blue (BSB, circles) and red (RSB, squares) sideband analysis pulses on a ground-state-cooled ion in $|\downarrow\rangle$ versus the detuning of the microwaves from the r_1 sideband transition. Both the cooling and the analysis pulses are performed using the oscillating gradient sidebands described in the text. Lines are fits giving $\bar{n} = 0.09(7)$.

data yields $\Omega_g/2\pi = 1.383(6)$ kHz, corresponding to a magnetic field gradient of 49.4(2) T/m along $\vec{r}_1$, in agreement with simulations [31].

We can use the resolved red sideband at $\delta \approx -(\omega_{r1} - \omega_g)$ to cool the r_1 mode, as shown in Fig. 4(b). Starting from a Doppler-cooled mean phonon occupation of $\bar{n} \approx 2$, we use a sequence of twelve 150 μs pulses with interleaved optical repumping to reach $\bar{n} = 0.09(7)$. The total cooling duration is ≈2.5 ms, more than an order of magnitude faster than previous demonstrations of microwave cooling using the static gradient scheme [33,34]. This speed-up is in part from using higher motional frequencies, which results in a lower initial thermal occupation after Doppler cooling.

For these experiments, we used a Blackman envelope [35] to adiabatically ramp the microwave pulse on and off over 10 μs. This pulse shaping allows us to operate with $2\Omega_\mu/(\omega_r - \omega_g) = 0.9$, and Ω_{sb} close to its maximum value of Ω_g. Compared to the static gradient scheme, our scheme allows $\Omega_{sb} = \Omega_g$ to be obtained for $2\Omega_\mu = \omega_r - \omega_g$ instead of a larger $2\Omega_\mu = \omega_r/2$. Thus, our scheme allows Ω_{sb} to be maximized for lower microwave currents. Larger Ω_g, and thus larger Ω_{sb}, can be achieved by increasing the current at ω_g in the trap electrodes. The maximum current will likely be limited by Joule heating in the trap electrodes. This heating is significantly lower for a current at megahertz frequencies than at gigahertz frequencies due to the larger skin depth. Furthermore, the magnitude of induced return currents in neighboring electrodes [36] is reduced for lower frequencies, yielding a larger gradient for a given applied current.

By moving ω_g closer to the motional frequency, we can maintain a given Ω_{sb} with lower microwave drive strength Ω_μ. This produces a smaller ac Zeeman shift, reducing decoherence due to fluctuations in Ω_μ. Reducing $\omega_r - \omega_g$ also increases the strength of higher-order sidebands that are proportional to $[\Omega_g/(\omega_r - \omega_g)]^n$ [28]. However, the finite impedance of the current-carrying electrodes gives rise to an oscillating potential on these electrodes at ω_g; the resulting electric field drives the ion's motion to an amplitude $\propto (\omega_r^2 - \omega_g^2)^{-1}$. Large-amplitude motion in surface-electrode traps samples increasingly anharmonic regions of the confining potential, and in extreme cases may cause the ion to leave the trap, setting a practical lower limit on the detuning of ω_g from ω_r. For the maximum measured Ω_g with B_g nulled at the ion, we measure the amplitude of this electric field to be ≈10 V/m [31,36]. The effects of electric fields at ω_g can be reduced for multiple ions by choosing differential motional modes which are not excited by a uniform electric field. Alternatively, one could directly compensate these oscillating electric fields using additional electrodes, or use trap designs which place the current-carrying electrodes beneath a metal layer [37] which shields electric fields more strongly than magnetic fields and their gradients.

In conclusion, we have demonstrated a new method for spin-motion coupling in trapped ions using microwaves and an oscillating magnetic field gradient with a frequency near that of a motional mode. This and other laser-free techniques for spin-motion coupling eliminate the photon scattering errors inherent in laser-based schemes. Moreover, our method addresses several technical limitations on the implementation of previous laser-free schemes. We demonstrate this method in a surface-electrode trap, where all control fields are generated using trap-integrated electrodes. Our scheme enables multiple sidebands to be produced using a single strong gradient and one weak microwave field for each sideband. The multiple sidebands required for Mølmer-Sørensen-type two-qubit gates, robust polychromatic two-qubit gates [38,39], or mixed-species operations [40] can then be implemented simply by adding relatively weak microwave fields. Recent theoretical investigations show that our technique is well suited for new dynamical decoupling schemes that reduce the complexity of microwave quantum logic gates in trapped ions, and that high-fidelity two-qubit gates should be achievable with realistic experimental parameters [41].

We thank T. R. Tan and S. C. Webster for helpful discussions, and M. Affolter and C.-W. Chou for comments on the manuscript. These experiments were performed using the ARTIQ control system. R. S., S. C. B., and D. T. C. A. are supported as Associates in the Professional Research Experience Program (PREP) operated jointly by NIST and the University of Colorado Boulder under Award No. 70NANB18H006 from the U.S. Department of Commerce, National Institute of Standards and Technology. This work was supported by ARO, ONR, and the NIST Quantum Information Program. Part of this work was performed under the auspices of the U.S. Department of Energy by Lawrence Livermore National Laboratory under Contract No. DE-AC52-07NA27344 with release number LLNL-JRNL-764019. This Letter is a contribution of NIST, not subject to U.S. copyright.

*raghavendra.srinivas@colorado.edu
†daniel.slichter@nist.gov

[1] D. J. Wineland, C. Monroe, W. M. Itano, D. Leibfried, B. E. King, and D. M. Meekhof, Experimental issues in coherent quantum-state manipulation of trapped atomic ions, J. Res. Natl. Inst. Stand. Technol. **103**, 259 (1998).
[2] R. Blatt and D. Wineland, Entangled states of trapped atomic ions, Nature (London) **453**, 1008 (2008).
[3] R. Blatt and C. F. Roos, Quantum simulations with trapped ions, Nat. Phys. **8**, 277 (2012).
[4] J. I. Cirac and P. Zoller, Quantum Computations with Cold Trapped Ions, Phys. Rev. Lett. **74**, 4091 (1995).
[5] C. Monroe, D. M. Meekhof, B. E. King, W. M. Itano, and D. J. Wineland, Demonstration of a Fundamental Quantum Logic Gate, Phys. Rev. Lett. **75**, 4714 (1995).
[6] K. Kim, M.-S. Chang, S. Korenblit, R. Islam, E. E. Edwards, J. K. Freericks, G.-D. Lin, L.-M. Duan, and C. Monroe, Quantum simulation of frustrated Ising spins with trapped ions, Nature (London) **465**, 590 (2010).
[7] B. P. Lanyon, C. Hempel, D. Nigg, M. Müller, R. Gerritsma, F. Zähringer, P. Schindler, J. T. Barreiro, M. Rambach, G. Kirchmair, M. Hennrich, P. Zoller, R. Blatt, and C. F. Roos, Universal digital quantum simulation with trapped ions, Science **334**, 57 (2011).
[8] J. W. Britton, B. C. Sawyer, A. C. Keith, C.-C. J. Wang, J. K. Freericks, H. Uys, M. J. Biercuk, and J. J. Bollinger, Engineered two-dimensional Ising interactions in a trapped-ion quantum simulator with hundreds of spins, Nature (London) **484**, 489 (2012).
[9] P. O. Schmidt, T. Rosenband, C. Langer, W. M. Itano, J. C. Bergquist, and D. J. Wineland, Spectroscopy using quantum logic, Science **309**, 749 (2005).
[10] F. Wolf, Y. Wan, J. C. Heip, F. Gebert, C. Shi, and P. O. Schmidt, Non-destructive state detection for quantum logic spectroscopy of molecular ions, Nature (London) **530**, 457 (2016).
[11] R. Ozeri, W. M. Itano, R. B. Blakestad, J. Britton, J. Chiaverini, J. D. Jost, C. Langer, D. Leibfried, R. Reichle, S. Seidelin, J. H. Wesenberg, and D. J. Wineland, Errors in trapped-ion quantum gates due to spontaneous photon scattering, Phys. Rev. A **75**, 042329 (2007).
[12] C. J. Ballance, T. P. Harty, N. M. Linke, M. A. Sepiol, and D. M. Lucas, High-Fidelity Quantum Logic Gates Using Trapped-Ion Hyperfine Qubits, Phys. Rev. Lett. **117**, 060504 (2016).
[13] J. P. Gaebler, T. R. Tan, Y. Lin, Y. Wan, R. Bowler, A. C. Keith, S. Glancy, K. Coakley, E. Knill, D. Leibfried, and D. J. Wineland, High-Fidelity Universal Gate Set for $^{9}Be^{+}$ Ion Qubits, Phys. Rev. Lett. **117**, 060505 (2016).
[14] S. Seidelin, J. Chiaverini, R. Reichle, J. J. Bollinger, D. Leibfried, J. Britton, J. H. Wesenberg, R. B. Blakestad, R. J. Epstein, D. B. Hume, W. M. Itano, J. D. Jost, C. Langer, R. Ozeri, N. Shiga, and D. J. Wineland, Microfabricated Surface-Electrode Ion Trap for Scalable Quantum Information Processing, Phys. Rev. Lett. **96**, 253003 (2006).
[15] K. R. Brown, A. C. Wilson, Y. Colombe, C. Ospelkaus, A. M. Meier, E. Knill, D. Leibfried, and D. J. Wineland, Single-qubit-gate error below 10^{-4} in a trapped ion, Phys. Rev. A **84**, 030303 (2011).
[16] T. P. Harty, D. T. C. Allcock, C. J. Ballance, L. Guidoni, H. A. Janacek, N. M. Linke, D. N. Stacey, and D. M. Lucas, High-Fidelity Preparation, Gates, Memory, and Readout of a Trapped-Ion Quantum Bit, Phys. Rev. Lett. **113**, 220501 (2014).
[17] U. Warring, C. Ospelkaus, Y. Colombe, R. Jördens, D. Leibfried, and D. J. Wineland, Individual-Ion Addressing with Microwave Field Gradients, Phys. Rev. Lett. **110**, 173002 (2013).
[18] D. P. L. Aude Craik, N. M. Linke, T. P. Harty, C. J. Ballance, D. M. Lucas, A. M. Steane, and D. T. C. Allcock, Microwave control electrodes for scalable, parallel, single-qubit operations in a surface-electrode ion trap, Appl. Phys. B **114**, 3 (2014).
[19] F. Mintert and C. Wunderlich, Ion-Trap Quantum Logic Using Long-Wavelength Radiation, Phys. Rev. Lett. **87**, 257904 (2001).

[20] M. Johanning, A. Braun, N. Timoney, V. Elman, W. Neuhauser, and C. Wunderlich, Individual Addressing of Trapped Ions and Coupling of Motional and Spin States Using rf Radiation, Phys. Rev. Lett. **102**, 073004 (2009).
[21] A. Khromova, C. Piltz, B. Scharfenberger, T. F. Gloger, M. Johanning, A. F. Varón, and C. Wunderlich, Designer Spin Pseudomolecule Implemented with Trapped Ions in a Magnetic Gradient, Phys. Rev. Lett. **108**, 220502 (2012).
[22] C. Ospelkaus, C. E. Langer, J. M. Amini, K. R. Brown, D. Leibfried, and D. J. Wineland, Trapped-Ion Quantum Logic Gates Based on Oscillating Magnetic Fields, Phys. Rev. Lett. **101**, 090502 (2008).
[23] C. Ospelkaus, U. Warring, Y. Colombe, K. Brown, J. M. Amini, D. Leibfried, and D. J. Wineland, Microwave quantum logic gates for trapped ions, Nature (London) **476**, 181 (2011).
[24] S. Weidt, J. Randall, S. C. Webster, K. Lake, A. E. Webb, I. Cohen, T. Navickas, B. Lekitsch, A. Retzker, and W. K. Hensinger, Trapped-Ion Quantum Logic with Global Radiation Fields, Phys. Rev. Lett. **117**, 220501 (2016).
[25] T. P. Harty, M. A. Sepiol, D. T. C. Allcock, C. J. Ballance, J. E. Tarlton, and D. M. Lucas, High-Fidelity Trapped-Ion Quantum Logic Using Near-Field Microwaves, Phys. Rev. Lett. **117**, 140501 (2016).
[26] M. Brownnutt, M. Kumph, P. Rabl, and R. Blatt, Ion-trap measurements of electric-field noise near surfaces, Rev. Mod. Phys. **87**, 1419 (2015).
[27] S. Ding, H. Loh, R. Hablutzel, M. Gao, G. Maslennikov, and D. Matsukevich, Microwave Control of Trapped-Ion Motion Assisted by a Running Optical Lattice, Phys. Rev. Lett. **113**, 073002 (2014).
[28] L. Förster, M. Karski, J.-M. Choi, A. Steffen, W. Alt, D. Meschede, A. Widera, E. Montano, J. H. Lee, W. Rakreungdet, and P. S. Jessen, Microwave Control of Atomic Motion in Optical Lattices, Phys. Rev. Lett. **103**, 233001 (2009).
[29] Y. M. Hu, W. L. Yang, Y. Y. Xu, F. Zhou, L. Chen, K. L. Gao, M. Feng, and C. Lee, Franck–Condon physics in a single trapped ion, New J. Phys. **13**, 053037 (2011).
[30] J. Welzel, A. Bautista-Salvador, C. Abarbanel, V. Wineman-Fisher, C. Wunderlich, R. Folman, and F. Schmidt-Kaler, Designing spin-spin interactions with one and two dimensional ion crystals in planar micro traps, Eur. Phys. J. D **65**, 285 (2011).
[31] See Supplemental Material at http://link.aps.org/supplemental/10.1103/PhysRevLett.122.163201 for detailed derivation of equations presented in text and simulations of magnetic fields and magnetic field gradients.
[32] Z. Meir, T. Sikorsky, R. Ben-shlomi, N. Akerman, M. Pinkas, Y. Dallal, and R. Ozeri, Experimental apparatus for overlapping a ground-state cooled ion with ultracold atoms, J. Mod. Opt. **65**, 501 (2018).
[33] S. Weidt, J. Randall, S. C. Webster, E. D. Standing, A. Rodriguez, A. E. Webb, B. Lekitsch, and W. K. Hensinger, Ground-State Cooling of a Trapped Ion Using Long-Wavelength Radiation, Phys. Rev. Lett. **115**, 013002 (2015).
[34] T. Sriarunothai, G. S. Giri, S. Wölk, and C. Wunderlich, Radio frequency sideband cooling and sympathetic cooling of trapped ions in a static magnetic field gradient, J. Mod. Opt. **65**, 560 (2018).
[35] F. J. Harris, On the use of windows for harmonic analysis with the discrete Fourier transform, Proc. IEEE **66**, 51 (1978).
[36] U. Warring, C. Ospelkaus, Y. Colombe, K. R. Brown, J. M. Amini, M. Carsjens, D. Leibfried, and D. J. Wineland, Techniques for microwave near-field quantum control of trapped ions, Phys. Rev. A **87**, 013437 (2013).
[37] J. Welzel, F. Stopp, and F. Schmidt-Kaler, Spin and motion dynamics with zigzag ion crystals in transverse magnetic gradients, J. Phys. B **52**, 025301 (2019).
[38] Y. Shapira, R. Shaniv, T. Manovitz, N. Akerman, and R. Ozeri, Robust Entanglement Gates for Trapped-Ion Qubits, Phys. Rev. Lett. **121**, 180502 (2018).
[39] A. E. Webb, S. C. Webster, S. Collingbourne, D. Bretaud, A. M. Lawrence, S. Weidt, F. Mintert, and W. K. Hensinger, Resilient Entangling Gates for Trapped Ions, Phys. Rev. Lett. **121**, 180501 (2018).
[40] T. R. Tan, J. P. Gaebler, Y. Lin, Y. Wan, R. Bowler, D. Leibfried, and D. J. Wineland, Multi-element logic gates for trapped-ion qubits, Nature (London) **528**, 380 (2015).
[41] R. T. Sutherland, R. Srinivas, S. C. Burd, D. Leibfried, A. C. Wilson, D. J. Wineland, D. T. C. Allcock, D. H. Slichter, and S. B. Libby, Versatile laser-free trapped-ion entangling gates, New J. Phys. **21**, 033033 (2019).